Bull. Soc. R. Sci. Liège, 2024, **93**(3), 129–155 *Peer-reviewed conference paper*
doi:10.25518/0037-9565.12302

Interacting Winds and Giant Eruptions in Massive Binaries

Amit KASHI[1,2]

[1] Department of Physics, Ariel University, Ariel 4070000, Israel
[2] Astrophysics, Geophysics and Space Science (AGASS) Center, Ariel University, Ariel 4070000, Israel
Correspondence to: kashi@ariel.ac.il

Paper presented at the 41st Liège International Astrophysical Colloquium on "The eventful life of massive star multiples," University of Liège (Belgium), 15–19 July 2024.

Abstract

Massive stars eject strong winds that affect their evolution. When in a binary system, their winds collide and emit radiation across the spectrum, providing an opportunity to study the stars and the interaction between them. There are many physical effects involved in the colliding-wind problem, and its complexity requires 3D numerical simulations. When one of the star is accreting the simulations become more complex. We present simulations of colliding winds in massive binary systems that include a detailed treatment of wind ejection, orbital motion, clumpiness, and other effects. These simulations are applied to different kinds of massive binaries that include LBVs, WR-stars, B[e] Supergiants, and O stars, in various primary–secondary combinations. We present results of simulations from some of the systems we studied. We show systematic simulations that were used to determine the general conditions that may lead to accretion onto the secondary star, and obtain the new *sub-Bondi–Hoyle–Lyttleton accretion*, with relationships between the mass accretion rate and the ratio of the stellar wind momentum. We also present recent results showing how the accreting secondary star responds to very high accretion rates, such as in giant LBV eruptions, and show how jets can suppress the accretion rate in such systems.

Keywords: stars: massive, stars: mass-loss, stars: winds, outflows, (stars:) binaries: general, accretion, accretion disks

1. Colliding Winds in Massive Stars

The evolution of very massive stars significantly differs from that of low-mass stars, with some aspects still not fully understood (e.g., Smartt, 2009; Georgy et al., 2017; Ekström, 2021; Farrell et al., 2022; Schneider et al., 2024). Massive stars exhibit unique physical processes, including strong winds and eruptive outbursts (e.g., Heger et al., 2000; Kudritzki and Puls, 2000; Puls et al., 2008; Maeder, 2009; Davidson and Humphreys, 2012; Vink, 2015; Kashi et al., 2016; Weis and Bomans, 2020). These stars are characterized by high mass loss rate

winds, which become more intense as they evolve off the main sequence (MS; e.g., Langer, 2012; Owocki, 2011, 2015; Vink, 2022; Curé and Araya, 2023).

Notably, many massive stars are part of binary and multiple systems. Using a population number synthesis code, Vanbeveren et al. (1998) found that the majority of massive stars are binaries, formed with orbital periods between 1 day and 10 years. They further suggested that most of these binaries experience interactions that affect their evolution. Mason et al. (2009) reported a 75% companion fraction for O stars in Milky Way clusters, while Sana et al. (2012) found that 70% of O stars have close companions, with about one-third potentially merging. Binary interactions significantly influence massive star evolution through mass transfer, common envelope evolution, tidal forces, and irradiation (e.g., Podsiadlowski, 2010; Smith, 2014; Eldridge et al., 2015; De Marco and Izzard, 2017; Eldridge, 2017; Schrøder et al., 2021; Zapartas et al., 2021; Schneider et al., 2024). Key evolutionary stages, such as the Luminous Blue Variable (LBV) and Wolf–Rayet (WR) stages, are now often attributed to binary evolution with mass exchange rather than single-star pathways (e.g., Kashi and Soker, 2010; Smith and Tombleson, 2015; Mahy et al., 2022). Studying massive stars thus requires attention to binary interactions.

For O stars and WR stars, the wind is optically thick and can maintain a steady-state due to bound-bound opacity from spectral lines (Puls et al., 2008; Owocki, 2010; Smith, 2014). Their mass loss aligns with the CAK line-driving model (Castor et al., 1975). LBVs lose mass via ordinary line-driving during quiescence but can have super-Eddington eruptions driven by continuum radiation (van Marle et al., 2008, 2009; Quataert et al., 2016). Clumping also affects mass loss rates by a factor of a few (Lépine and Moffat, 1999; Nugis and Lamers, 2000; Puls et al., 2006; Oskinova et al., 2007; Sundqvist et al., 2010; Hainich et al., 2014).

In binary systems with two stars ejecting winds, these winds collide, forming a colliding-wind structure (CWS) (e.g., Usov, 1992; Stevens et al., 1992; Eichler and Usov, 1993). The CWS typically has an axis-symmetric conical shape that thickens away from its apex. The apex is usually near this line, divided by a contact discontinuity with shock waves on either side. The shocked gas flows asymptotically along the cone's sides close to the stars, where we focus our simulation and discussion. The primary parameter influencing the contact discontinuity shape and the CWS is the momentum ratio of the winds $\eta = (\dot{M}_2 v_2)/(\dot{M}_1 v_1)$, where $\dot{M}_2$ and v_2 are respectively the mass loss rate and the wind velocity of the secondary star, and $\dot{M}_1$ and v_1 are those of the primary. The star with the greater wind momentum is the primary. If the stars were stationary, the CWS would be symmetric with respect to the line connecting their centers. However, due to their orbital motion, the CWS becomes curved, which can lead to differences between the leading and trailing arms and shift the apex away from the line connecting the two stellar centers. Depending on the momentum ratio and the velocity ratio of the winds to the orbital velocity, the structure can be conical or spiral. When the ratio between the orbital velocity and the wind velocity is large, the shape of the CWS can change, often resembling a spiral further from the stars.

The study of these systems stretches beyond our Galaxy. Several massive colliding-wind systems have been detected in the Large Magellanic Cloud (LMC) and Small Magellanic Cloud

(SMC). Examples include Melnick 34 (Mk 34; Brey 84, Pollock et al. 2018; Tehrani et al. 2019), Melnick 33Na (Cl* NGC 2070 MEL 33N; Bestenlehner et al. 2022), and V.R 144 (RMC144; Shenar et al. 2021) in the LMC's 30 Doradus region. Williams et al. (2021) observed a dust formation episode in the WR star HD 38030 in the LMC, indicating an O star companion. In the SMC, HD 5980, a multiple system, contains an LBV primary with a WR secondary (Koenigsberger et al., 2014; Nazé et al., 2018; Hillier et al., 2019). Garofali et al. (2019) discovered N604-WRX ([GLM2019] N604 WRXc), the first colliding-wind binary in M33, consisting of a WC4 star and an O star companion.

Analytical descriptions of colliding winds are feasible only when they are adiabatic, as radiative cooling introduces instabilities and inhomogeneities (Stevens et al., 1992; Usov, 1992). Non-linear growth of instabilities, such as the Nonlinear Thin Shell Instability (NTSI; Vishniac, 1994), makes the analytical description of the problem difficult. Numerical simulations are thus essential for addressing colliding-wind problems. Early 3D simulations for γ^2 Vel and WR 140 showed the formation of the pinwheel structure, X-ray variability, and instability and clumping in the winds (Folini and Walder, 2000, 2002; Walder and Folini, 2000, 2002, 2003).

As an example of modern 3D simulations a colliding-wind system we chose to present Mk 34. The binary system consists of two WN5h stars located in the 30 Doradus region of the LMC. It has a high eccentricity $e = 0.68$ and an orbital period $P \simeq 155$ days (Pollock et al., 2018), with mass estimates of 139–147 $M_\odot$ and 127–136 $M_\odot$ for its components (Tehrani et al., 2019), making it one of the most massive binary systems known. Mk 34 is characterized by strong X-ray emissions, that show high-amplitude orbital variability, exceeding even η Carinae (Pollock et al., 2018). The wind momentum ratio of Mk 34 is $\eta = 0.69$, and the winds of both stars are adiabatic which makes it unlikely to experience accretion close to periastron. Analytical estimates of the wind pressure balance show that a stable solution exists along the entire orbit, including during periastron passage. Figures 1 and 2 show our simulations of the the Mk 34 system close to periastron and apastron passage. The shape of the CWS changes between a conical shape and a spiral. Indeed the simulations show that there is no accretion at any point during the orbital period. In the following we will see other systems that do show accretion, and discuss its implications.

2. Simulating Colliding Winds with Accretion

Simulations of accretion onto compact objects have evolved from 2D to 3D (e.g., Soker et al., 1986; Ishii et al., 1993; Ruffert, 1994; Nagae et al., 2004). *Accretion against wind* is rarer and more challenging to simulate. In this case the arriving gas experiences an opposing force by the wind and radiation of the secondary.

η Carinae was the first system where accretion against wind was suggested and tested (Soker, 2005). Parkin et al. (2011) and Madura et al. (2012) simulated the colliding winds in η Carinae and described a collapse of the shocked wind onto the secondary during periastron passage. They did not discuss whether the primary wind is accreted onto the secondary, which would suggest accretion, or somehow immediately expelled upon reaching it. In either case,

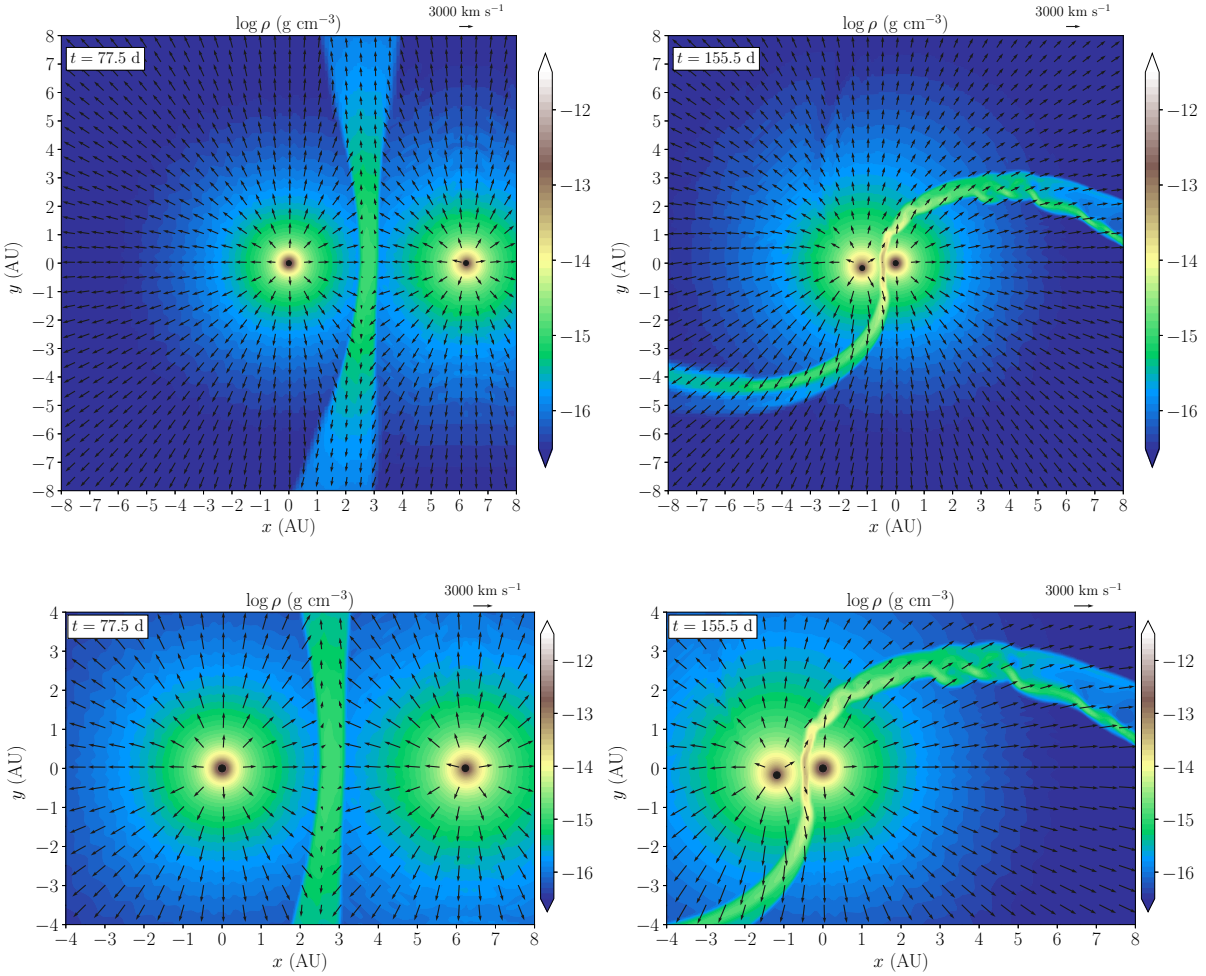

Figure 1: Simulations of the colliding-wind binary Mk 34. (*Top left*) Density at apastron, showing a conical shell with a wide angle. (*Top right*) Density at periastron, showing a transition into a spiral. (*Bottom*) Zoom-in into the top panels. There is no accretion at any point during the orbital period, as the two stars have comparable wind momenta.

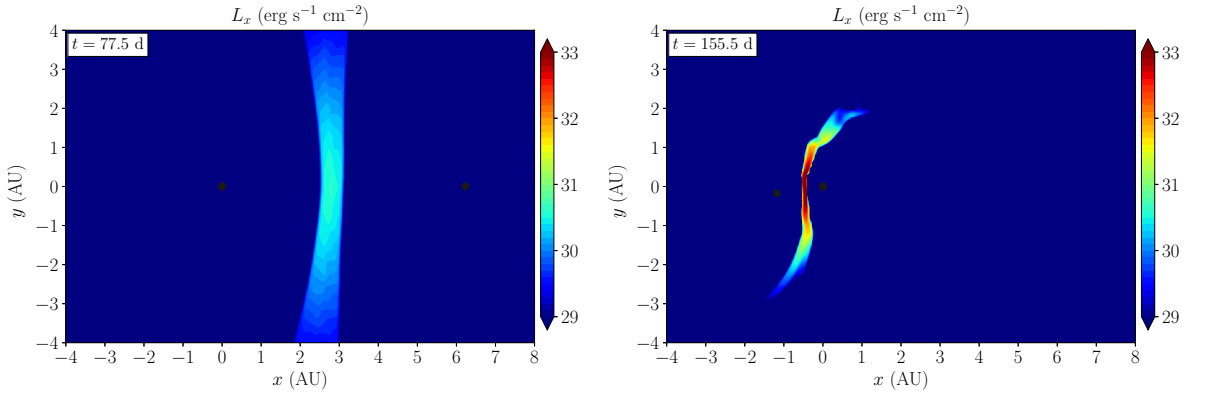

Figure 2: Simulations of the colliding-wind binary Mk 34. (*Left*) X-ray emission at apastron. (*Right*) X-ray emission at periastron.

their results agree that no stable colliding-wind solution exists close to periastron, and that the CWS is destroyed. Hydrodynamical simulations by Akashi et al. (2013) found dense clumps formed by instabilities in the primary wind of η Carinae, which then hit the secondary close to periastron passage. Kashi (2017) and Kashi (2019) showed that such filaments get accreted onto the secondary, and that radiative braking or inhibition did not stop the accretion.

Kashi (2020) employed hydrodynamic simulations to study the colliding winds in the massive binary system HD 166734. The system comprises a primary star with a mass $M_1 \approx 39.5\,M_\odot$ and a secondary star with a mass $M_2 \approx 30.5\,M_\odot$, with an orbital period $P \approx 34.538$ days. The code simulated the hydrodynamics of the colliding winds at high resolution, allowing instabilities such as the NTSI (Vishniac, 1994) to seed and evolve. These instabilities were time-dependent and varied throughout the orbital motion. The system's high eccentricity ($e \approx 0.618$) led to a fundamental difference between the apastron and periastron phases. Approximately two days before periastron passage, the primary star's wind began to be accreted onto the secondary star, and this accretion continued until about 10 days after periastron. As the stars moved apart, the secondary wind reinstated itself, and the system returned to its previous state, characterized by a colliding-wind structure similar to that observed before periastron.

The close orbit of HD 166734 led to significant influence from the secondary star's gravity, resulting in accretion occurring over a large fraction of the orbit. The accretion observed in the simulation was a result of the dynamic interactions modeled and was not assumed a priori. In total, a mass of approximately $1.3 \times 10^{-8}\,M_\odot$ was accreted during each orbital cycle. The expected X-ray emission was calculated through detailed post-processing. In this computation, the orientation proposed for the system by Nazé et al. (2017) was used, yielding qualitatively similar results. It is however possible that adjustment of the parameters of the system could have provided better fit to the light curve and other observations.

It is practically impossible to adjust a large set of stellar, wind and orbital parameters to obtain a better match, as each set requires a complete simulation which is computationally very expensive. In this case, it can be useful to run a large set of high resolution 3D numerical that separates each physical effect and measures how each of the parameters affects the structure and hydrodynamic properties of the CWS.

Kashi et al. (2022) ran a numerical experiment of ejecting winds in a massive colliding-wind binary system, and quantifying the accretion onto the secondary star under different primary mass loss rates. The goal was to assess the accretion-against-wind problem and quantify the effect of the secondary's wind in reducing the accretion rate below the classical Bondi–Hoyle–Lyttleton (BHL) value that assumes no wind from the secondary. We adopt a binary system comprising a LBV as the primary and a WR star as the secondary, with masses $M_1 = 80\,M_\odot$ and $M_2 = 20\,M_\odot$. For the fiducial run, the primary's mass loss rate is $\dot{M}_1 = 3 \times 10^{-4}\,M_\odot\,\mathrm{yr}^{-1}$, with a wind terminal velocity value of $v_{1,\infty} = 500\,\mathrm{km\,s}^{-1}$ and radiative acceleration corresponding to $\beta = 1$; the secondary's mass loss rate is $\dot{M}_2 = 10^{-5}\,M_\odot\,\mathrm{yr}^{-1}$, with a wind terminal velocity value $v_{2,\infty} = 3000\,\mathrm{km\,s}^{-1}$ and an acceleration parameter $\beta = 0.8$. We initiate the simulation with two smooth winds (homogeneous without clumps). The momentum ratio is $\eta = 0.2$, but as the winds collide before reaching their terminal velocity, the effective momentum ratio varies with

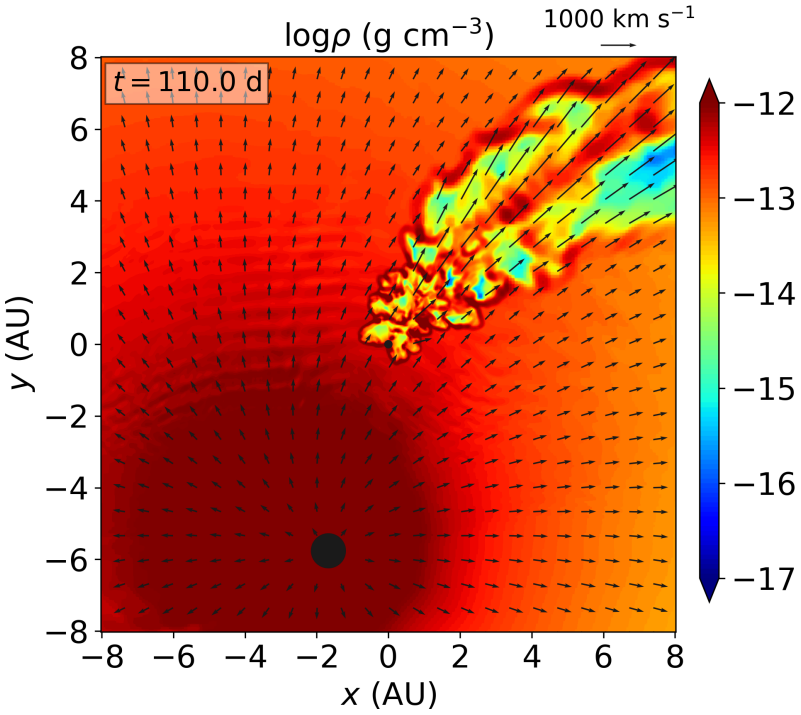

Figure 3: A simulation with a $80 M_\odot$ primary and a $20 M_\odot$ secondary on a circular orbit with a radius $a = 6$ AU. The momentum ratio of the two winds is almost as low as the threshold where the secondary's wind is shut. This situation is representative for a giant eruption with a relatively low mass loss or a secondary with a strong wind of its own. Behind the secondary (marked by the small black circle at the center of the grid) a turbulent wind is formed. In such a case the accretion is sub-BHL and the accretion rate is highly fluctuating. An accretion disk is not formed under these conditions as there is insufficient angular momentum.

location. By increasing the primary's mass loss rate, we effectively reduced the momentum ratio η and check the amount of accreted mass on the companion as a result. The primary's wind collided with the pre-existing CWS and alters its shape to a smaller opening angle. The side of the CWS facing the secondary exhibits strong instabilities, forming dense clumps and filaments. The secondary's gravity pulls these filaments, and some of them get accreted onto the secondary. The secondary's wind attempts to flow against the incoming gas, forming bubbles. We then continued to run a large set of simulations, varying the mass loss rate of the LBV to obtain different values of wind momentum ratio. An example for a limiting case where the secondary's wind is almost extinguished is shown in Fig. 3.

Figure 4 shows the accretion rate both in physical and BHL accretion rate units. The top and bottom panels of Fig. 4 are updated versions of Figs. 11 and 14 from Kashi et al. (2022), and include the results for two additional simulations. For $\eta > 0.05$ there was no accretion (Region (i) in Fig. 4); for smaller values, accretion occurs while the wind of the secondary is still dominant, and we get *sub-BHL* accretion (Region (ii)). The instabilities in the CWS form clumps that have a velocity component in the direction of the flow (namely, along the sides of

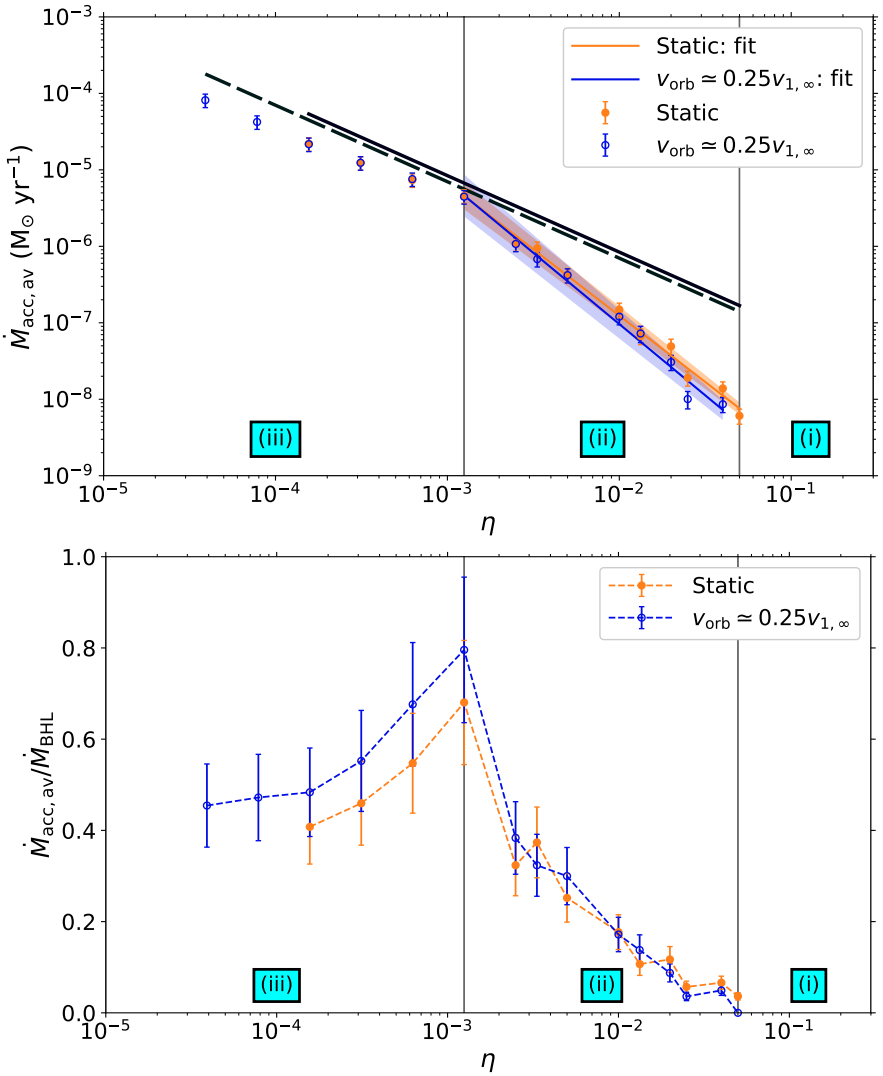

Figure 4: Results of 30 simulations of accretion at different secondary to primary wind momentum ratios (η). (*Top*) Time-averaged accretion rates. (*Bottom*) Time-averaged accretion rates in BHL units. Region (i) – No accretion: for $\eta > 0.05$ the secondary wind pushes away all the primary wind material so there is a well-defined colliding-wind structure with a conical shape and no accretion. Region (ii) – *Sub-BHL Accretion*: For $0.01 < \eta < 0.05$ there is a transition region, in which accretion is very sporadic. Mass can occasionally be accreted, but for most of the time the secondary's wind and radiation prevent accretion. For $0.001 < \eta < 0.01$, accretion occurs most of the time. The accretion rate and the accretion duty cycle are larger as η decreases. The accretion rate satisfies a power-law relation with a slope of about -1.8. Region (iii) – BHL accretion: for $\eta \lesssim 0.001$ the accretion becomes continuous in time and the accretion rate is close to BHL. We find that the fraction is in the range 0.4–0.8. The two left-most points are results of new simulations with extremely low η, indicative of a secondary with almost no wind at all.

the CWS) but also have the acceleration of the secondary. Depending on the parameter values, some of the clumps can be pulled towards the secondary and get accreted. As long as the wind of the secondary is able to push part of the clumps away and prevent them from being accreted, the accretion follows a power law of about $\dot{M}_{\rm acc} \propto \eta^{-1.73}$ for static stars, and steeper $\dot{M}_{\rm acc} \propto \eta^{-1.86}$ when orbital motion is included.

For very low η the secondary wind almost does not exist. Accretion under such conditions (Region (iii) in Fig. 4) is directly onto the secondary as there is no colliding-wind structure, but instead a geometry that resembles BHL accretion, with some differences: the wind velocity vectors are not parallel and its value is not constant and exposed to the stellar radiation. We obtain an accretion rate of about 0.4–0.8 times the BHL accretion rate, in agreement with the early results of Livio et al. (1986).

3. Colliding Winds with Jets

The role of jets in colliding wind binaries can be explained by using the interaction between the winds of the primary and the secondary of η Carinae. The system is a binary (Damineli et al., 2000; Davidson and Humphreys, 1997) composed of a very massive LBV (the primary) with a mass M_1 estimated at 120–170$M_\odot$ (Hillier et al., 2001; Davidson and Humphreys, 2012; Kashi and Soker, 2010, 2016), and a hotter and less luminous companion (the secondary) with a mass M_2 estimated at 30–80$M_\odot$ (Kashi and Soker, 2010, 2016), which was suggested to be in its Wolf–Rayet stage (e.g., Hirai et al., 2021). The system is a colliding-wind binary with an orbital period $P_0 \simeq 5.54$ years and large eccentricity $e \simeq 0.9$ (e.g., Davidson et al., 2017), resulting in large differences in the wind collision interface when approaching periastron passage, due to the higher orbital velocity and the close proximity of the stars. The LBV has undergone at least two major eruptions: the Great Eruption (GE) in ca. 1839–1858 which created the bipolar Homunculus nebula which contains 10–45$M_\odot$ (Gomez et al., 2010; Morris et al., 2017), and the Lesser Eruption (LE) which took place between 1887 and 1895, was much less energetic (Humphreys et al., 1999) and ejected only 0.1–1$M_\odot$ (Kashi and Soker, 2010). Prior to periastron passage, η Car's spectral lines, which serve as probes of the dynamics of the two stars and their winds, change their profiles. These changes, together with rapid variations in various bands, from radio to X-ray, around periastron passages is known as "the spectroscopic event" (e.g., Martin et al., 2006; Soker and Behar, 2006; Hamaguchi et al., 2007; Damineli et al., 2008; Kashi and Soker, 2007, 2008; Davidson and Humphreys, 1997, 2012; Mehner et al., 2015; Richardson et al., 2015; Kashi et al., 2021; Grant et al., 2023).

Counting the periastron passages back in time simply by subtracting a natural multiplicity of P_0, one finds that the LE started very close to periastron. The beginning of the LE just as periastron passage occurred led Kashi and Soker (2010) to assume that giant LBV eruptions are triggered by periastron passages of a binary companion. For that to occur, the primary must already be unstable, but it is the secondary that makes the eruption so energetic, and prolongs its duration in subsequent periastron passages (Kashi, 2010). A significant eruption does not happen during every periastron passage because the primary star must already be in an unstable

condition for the secondary star to be able to trigger a major eruption. For the same reason, an eruption does not happen during every periastron passage.

The accretion model is also supported by bipolar nebulae that are present around about half of LBVs either in the shape of an hourglass or polar caps (Weis, 2011). In the accretion model the bipolarity of the nebula is explained by an *accretion disk* that forms around the secondary, and induces *two opposite jets*. The jets interact with the CSM and create a bipolar nebula (Soker, 2001). In η Carinae, this process might have happened twice, creating the Homunculus nebula during the GE, and the inner little Homunculus during the LE (Ishibashi et al., 2003; Abraham et al., 2014; Gull et al., 2024).

If the angular momentum of the accreted gas is significant, a disk can be formed. In some cases, when the periastron interaction time is shorter than the viscosity timescale of a disk, the disk will not flatten, and a thick accretion belt can form instead (Kashi and Soker, 2009). The disk or the belt can be accompanied by two polar jets that either blow through the nebula and create caps, or, if they are wider, can create an hourglass shaped nebula. Jets may also form even when a temporary disk is created close to periastron passage. Such a disk can be dissipated by the restored winds of the secondary star. The accreted material forms a thick accretion belt around the secondary η Carinae at every periastron passage (Kashi and Soker, 2009). The winds are being restored in a duration of a few months after a few$\times 10^{-6} M_{\odot}$ have been accreted during periastron passage.

We have simulated an example of a massive colliding wind binary system with jets. As our simulations do not include magnetic fields, the launch of jets has to be done manually. Figure 5 shows two slices of a 3D representation of a colliding wind system with jets. The material reaches the secondary and accretes, and two opposite jets are launched conserving the accretion energy. The jets interact with the material arriving from the primary. The collision deflects the jets in a direction away from the primary. The jets prevent part of the primary's gas from reaching the secondary, thereby effectively reducing the accretion rate onto the secondary. Figure 6 shows a comparison between the accretion rates of two similar experiments, with and without jets. It can be seen that the accretion rate is reduced by about a factor of three. A more detailed study of the effects of jets in accreting colliding-wind binaries and a quantitative description of the effect of jets on accretion is still ongoing.

4. The Effect of Accretion on the Accreted Star

In our simulations in Kashi and Michaelis (2021) and Kashi et al. (2022) we did not modify the stellar atmosphere as a result of accretion. Accretion at a very high rate can lead to a reduction in the effective temperature of the star and in turn weaken its wind, as suggested by Kashi and Soker (2009) for accretion close to the periastron passage of η Carinae. This effect was later obtained in simulations (Kashi, 2017). Kashi et al. (2016) simulated the state changes triggered by a giant eruption using two methods that conserve total energy: (1) synthetically removing outer layers while decreasing the energy in the inner layers, and (2) synthetically transferring energy from the core to the outer layers, which naturally leads to mass ejection.

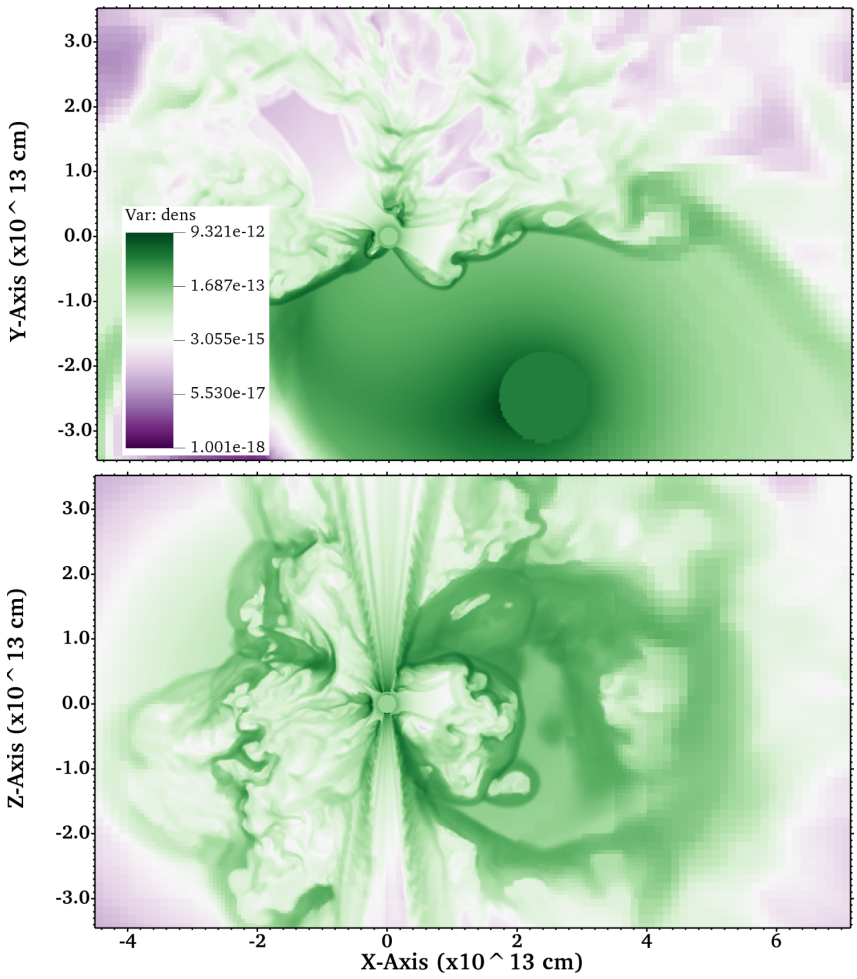

Figure 5: A simulation of an LBV and a secondary massive star in an eccentric orbit, creating a temporary accretion disk that launches jets. The jets prevent from part of the material to arrive to the secondary, by that creating a negative feedback effect that reduces the accretion rate, and helps the secondary wind to dissipate from the disk and restore. (*Top*) Orbital plane: the secondary is located at the origin, the primary orbits the secondary with periastron on the left side of the secondary. Note that the density values within the stars is arbitrary, as the stars are not modeled. (*Bottom*) Edge-on view showing the jets. The jets create a bipolar cavity that clears the primary gas, by that reducing the accretion rate.

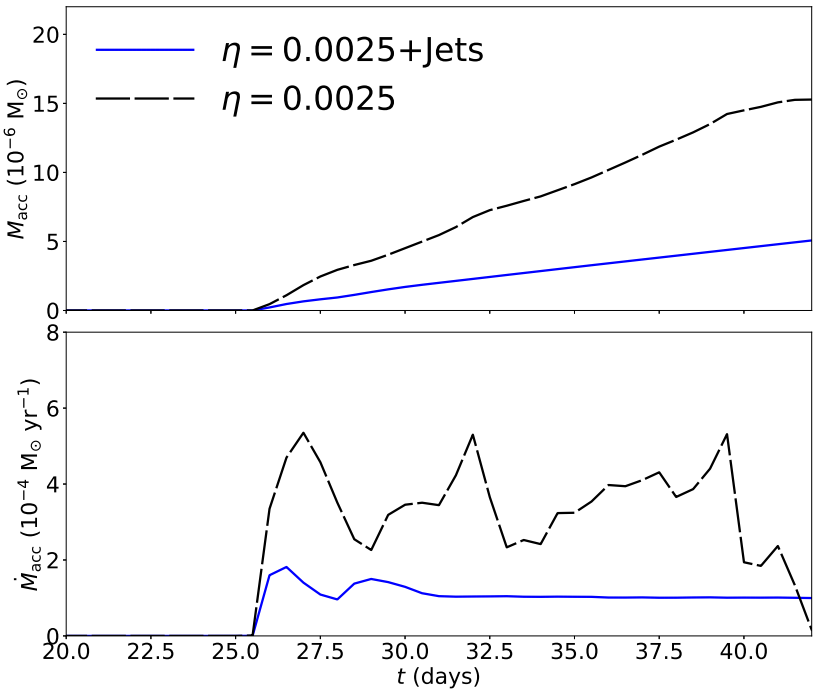

Figure 6: A simulation with a $80\,M_\odot$ primary and $20\,M_\odot$ secondary at $a = 6$ AU. The momentum ratio of the two winds is similar for both simulations ($\eta = 0.0025$). When jets are launched they create a negative feedback effect that reduces the mass accretion rate. (*Top*) Total accreted mass. (*Bottom*) Mass accretion rate.

Typically, the star developed a wind with a velocity of around few times $100\,\mathrm{km\,s^{-1}}$ and an initial mass loss rate of about $0.1\,M_\odot\,\mathrm{yr}^{-1}$, which gradually decreased. This outflow was driven by κ-mechanism radial pulsations, and lasted for about 200 years, similar to the time it took η Carinae to recover from the GE.

In Mukhij and Kashi (in prep.) we illustrate how a massive companion star in a binary system, where the primary star undergoes a Giant Eruption, reacts to the rapid accretion of gas from the primary star. The rate of mass accretion is influenced by the mass loss of the erupting star, the separation within the binary system, and the radiation field of the accretor, which can reduce the amount of material reaching it. We adopted a simplified approach with a constant accretion rate to demonstrate how the star responds to the accumulation of mass in its outer layers, which leads to changes in its surface stellar parameters. We employed the 1D stellar evolution code MESA (Paxton et al., 2013, 2015) to track the evolution of a $3\,M_\odot$ star. Figure 7 shows how the star evolves on a Hertzsprung–Russell (HR) diagram from the Zero Age Main Sequence to the end of the helium-burning phase without any accretion process. Simulations were run with different accretion rates starting from point B, applying accretion to the star's outer layers over 20 years. The star exhibited different responses to lower and higher accretion rates: for high accretion rates, $\gtrsim 10^{-2}$ and $10^{-1}\,M_\odot\,\mathrm{yr}^{-1}$, the star became cooler, whereas for lower rates, it remained on the hotter side of the HR diagram during accretion.

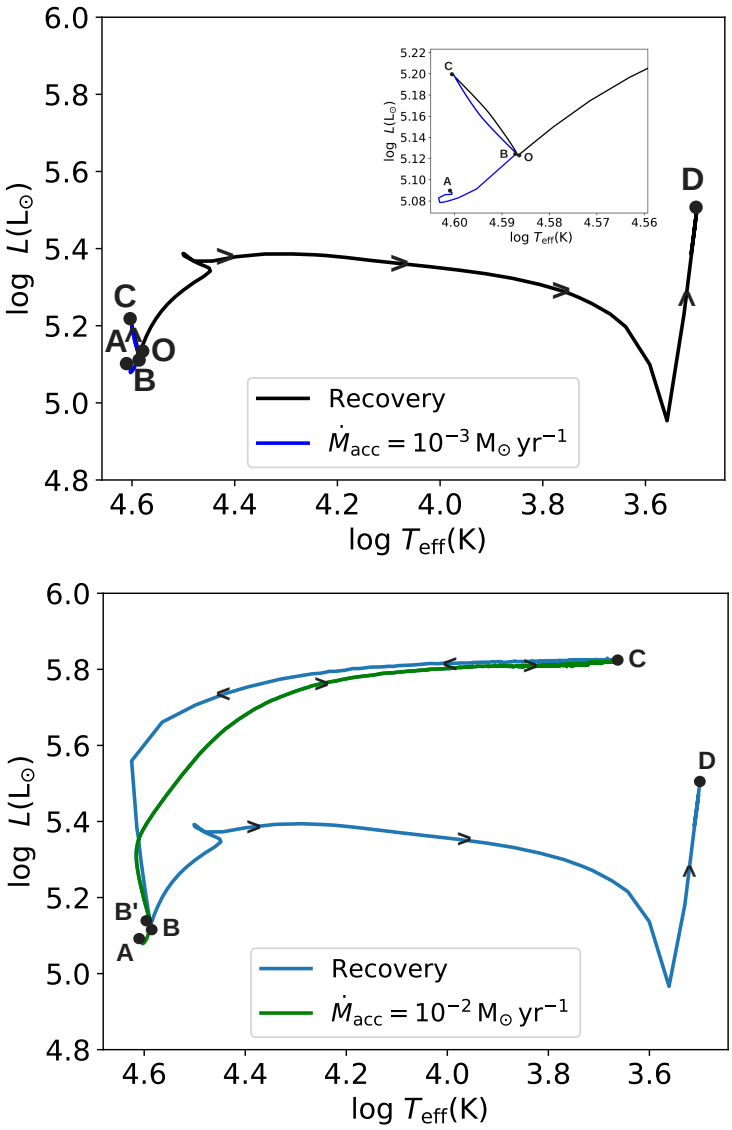

Figure 7: Stellar tracks of luminosity and temperature (HR diagram) of a $30\,M_\odot$ for accretion rates are obtained using MESA. (*Top*) Evolutionary track for an accretion rate of $10^{-3}\,M_\odot\ {\rm yr}^{-1}$. The tracks from points B to C show the accretion phase, and tracks from points C to O and O to D show the recovery phase of the star. In the recovery scenario, the track from point C to O represents the loss of gravitational energy through stellar winds. As a result, there is a vertical drop in the luminosity for the lower accretion rates. This vertical drop mechanism occurs due to the mass loss by stellar wind, which is caused by the high temperature at point C. (*Bottom*) Evolutionary track for an accretion rate of $10^{-2}\,M_\odot\ {\rm yr}^{-1}$. During the accretion phase, a star with a high accretion rate experiences flashes. As the star transitions to the recovery phase after completing the accretion, it shifts to the hot side of the HR diagram and continues to evolve. The track from point B to C shows the accretion phase, and from C to D (from point C to B', and B' to D) the recovery phase.

During the accretion phase, a star with a high accretion rate experienced flashes. As the star transitioned to the recovery phase after completing the accretion, it shifted to the hot side of the HR diagram and continued to evolve. For the lower accretion rate, due to high temperature, the star underwent stellar wind mass loss shortly after accretion, expelling material and causing a drop in luminosity. We observed that in the early days of accretion, the luminosity and the effective temperature increased rapidly. This phenomenon is due to gravitational energy from the additional material being converted into thermal energy, thus raising the specific luminosity and the temperature in the star's outer layers. The total energy added during this phase increased the star's luminosity. However, not all of this energy was radiated outwards, contributing to the increase in luminosity. For higher accretion rates, approximately 46% of the added energy enhanced luminosity, while for lower accretion rates, only about 23% was radiated outward, increasing the luminosity. As the star evolved further, its luminosity and radius stabilized. while the temperature dropped due to the dominance of the outer layers at high accretion rates. Additionally, our simulations revealed that for high accretion rates the compression caused by the added material in the outer layers also became significant, leading to fluctuations in luminosity during the initial days of the accretion phase.

Observational testing of the results is difficult, as most of the light comes from the LBV rather than from the accreting secondary star. The ejection of mass makes the system obscured, and it is only after the dissipation of the material, which takes decades to centuries, that the system will be revealed. Both the primary and the secondary change after the eruption, but high-excitation lines that vary along the orbit should be able to reveal if the secondary remained hotter or cooled. The timescale for the ejection of the mass is comparable to the time of recovery from the accretion, so by the time it becomes visible, the secondary might already have returned to its hotter state. Also, in cases where jets are launched, the star is expected to remain hot rather than to expand (Bear and Soker, 2024). Together with the rarity of these systems, there is currently no other example than η Carinae for which the secondary is hot.

5. Accretion in B[e]SG Systems

In this section we extend the accretion model to explain certain phenomena in binary systems containing B[e] supergiant stars (B[e]SGs) as primaries. B[e]SGs are rare stars, and only a few tens of them are known to date. They exhibit optical spectra with strong Balmer emission lines, low-excitation permitted emission lines of predominantly low-ionization metals, and forbidden emission lines, as well as strong infrared excess in their spectrum, and few if any apparent absorption lines (e.g., Allen and Swings, 1976; Zickgraf et al., 1986, 1996; Zickgraf, 2006; Aret et al., 2016; Humphreys et al., 2017; Oudmaijer and Miroshnichenko, 2017; Kraus, 2019). The rarity of B[e]SGs suggests that they may represent a brief transitional phase in the evolution of certain massive stars, characterized by intense mass loss (e.g., Kraus et al., 2021). B[e] stars are also associated with large-scale gas structures, ranging from spherical and ring nebulae to spiral arms, partial spirals, and bipolar or unipolar lobes (e.g., Marston and McCollum, 2008). Radial velocity measurements of the circumbinary material around B[e] stars suggest an outflowing velocity component (Kraus et al., 2010). Observations indicate that this

circumstellar gas is often arranged in multiple rings, arcs, or spiral arm-like structures (Torres et al., 2018; Kraus et al., 2016; Maravelias et al., 2018; Liimets et al., 2022).

Some B[e]SGs were suggested to be in binary systems, and in this case the circumstellar disk is in fact a circumbinary disk. It is difficult to explain the asymmetries in the circumstellar medium of B[e]SGs with a single star, since their stellar evolution models predict small rotation rates for blue supergiants at the observed position of B[e]SGs in the HR diagram (Georgy et al., 2017). Thus, the similarity between the B[e]SGs, LBVs and FS CMa might support a binary origin for the B[e]SGs as well.

GG Carinae (HD 94878) is a well-studied confirmed binary B[e]SG system (Swings, 1974; Gosset et al., 1985; Brandi et al., 1987; Machado et al., 2004; Kraus et al., 2013; Porter et al., 2021, 2022) with a high-mass, high-luminosity primary ($M_1 = 24 \pm 4 M_\odot$, $\log(L_1/L_\odot) = 5.26 \pm 0.19$; Porter et al., 2021) and surrounded with a complex circumstellar environment. However, its unusual behavior on both short and orbital timescales suggests it may be an atypical system that undergoes enhanced mass transfer and accretion from the primary to the secondary at periastron (Porter et al., 2021). Previous evolutionary studies of GG Carinae typically assumed that its two components evolved as pseudo-single stars (Kraus et al., 2013; Kraus, 2019). In contrast, Porter et al. (2021) proposed a different perspective, modeling the system as a binary with interacting components.

In Kashi (2023) we simulated the hydrodynamics of the wind flow of GG Carinae and obtained the mass accretion rate onto the secondary and the observed light curve. We find that the accretion takes a geometric form that resembles inhomogeneous BHL accretion (Livio et al., 1986). The primary wind flows from both sides of the secondary, and, focused by its gravity, into a curved tail. Part of the accretion tail flows towards the secondary and gets accreted, and part of it flows outwards and creates a spiral structure. Accretion also takes place from other directions, but at a lower rate. After periastron passage, a clear dense accretion disk is obtained around the secondary. We identify an effect related to the orbital motion of the two stars, whereby the accretion tail is severed by the primary star; we refer to this as the *Lizard Autotomy Effect*. A representation of this effect is shown in Fig. 8. As part of this effect, the primary star re-accretes wind that it had previously ejected. The Lizard Autotomy Effect results in an outwardly expanding spiral shell composed of broken segments.

We suggested that such tails exists in other B[e]SGs systems and can be the source of the circumstellar material observed in such systems. The accretion onto the secondary also forms a disk around the secondary (not a circumbinary disk) near periastron that later disperses. Some of the gas later remains and forms a dense filament. The formation of such a disk can be accompanied by the launching of two opposite jets perpendicular to the plane of the disc. These two jets can push ambient gas and form a bipolar structure. Such bipolar structures were observed around some B[e]SGs (Torres et al., 2018; Liimets et al., 2022).

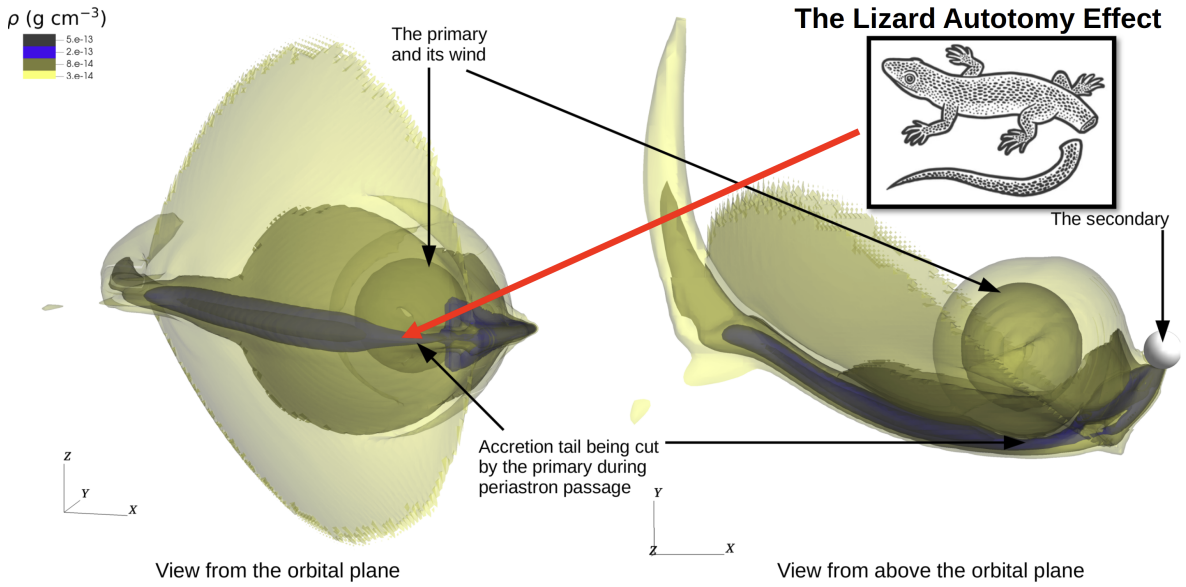

Figure 8: 3D view of the GG Carinae binary system close to periastron passage. There is a dense tail behind the secondary, part of which is an accretion tail towards the secondary and part is outflowing away from it. The secondary takes a sharp elliptical turn close to periastron, and as a result the close primary and its wind cut the tail and create a gap in the tail – the Lizard Autotomy Effect. The process repeats at each periastron passage, creating an outflowing spiral with gaps.

6. Conclusions

We discussed a physical system that has a number of components and effects:

1. Two massive stars in a binary system, possibly eccentric, both have winds that collide and create a hot shocked region that emits in the X-ray range.

2. The star which has the wind with the weaker momentum (the secondary) accretes the wind of the other star; accretion can be either continuous, intermittent, or occur only during the part of the orbit that is close to periastron.

3. The accretion is accompanied by a total or partial destruction of the colliding wind structure which emits the X-rays.

4. An accretion disk or a thicker accretion belt can form around the secondary.

5. The accretion disk may block part of the ionizing radiation of the secondary, which affects the emission of high-ionization lines from other parts of the system.

6. The accreted wind changes the photospheric solution of the star, and increase its luminosity.

7. Jets can be launched from the disk, creating a negative feedback effect that reduces the accretion rate or expedites the termination of the accretion phase. They can also form a bipolar nebular structure.

We presented simulations of colliding winds with accretion, focusing on a structured set of models and specific binary systems. Investigating these systems and their various effects enhances our understanding of stellar winds, binary evolution, and accretion processes. Simulations are an essential tool in this research, enabling the incorporation of more detailed physics and improving the accuracy of results when applied to observed systems.

Acknowledgments

The author would like to thank the conference organizers for the opportunity to present the work in this very interesting conference, and an anonymous referee for helpful comments. We acknowledge support from the R&D Authority at Ariel University. We acknowledge the Ariel HPC Center at Ariel University for providing computing resources that have contributed to the research results reported in this paper.

Further Information

Author's ORCID identifier

0000-0002-7840-0181 (Amit KASHI)

Conflicts of interest

There are no conflicts of interest.

References

Abraham, Z., Falceta-Gonçalves, D., and Beaklini, P. P. B. (2014) η Carinae Baby Homunculus uncovered by ALMA. *ApJ*, **791**(2), 95. https://doi.org/10.1088/0004-637X/791/2/95.

Akashi, M. S., Kashi, A., and Soker, N. (2013) Accretion of dense clumps in the periastron passage of η Carinae. *NewA*, **18**, 23–30. https://doi.org/10.1016/j.newast.2012.05.010.

Allen, D. A. and Swings, J. P. (1976) The spectra of peculiar Be star with infrared excesses. *A&A*, **47**(2), 293–302. https://ui.adsabs.harvard.edu/abs/1976A&A....47..293A.

Aret, A., Kraus, M., and Šlechta, M. (2016) Spectroscopic survey of emission-line stars – I. B[e] stars. *MNRAS*, **456**(2), 1424–1437. https://doi.org/10.1093/mnras/stv2758.

Bear, E. and Soker, N. (2024) On the response of massive main sequence stars to mass accretion and outflow at high rates. arXiv e-prints: arXiv:2407.03182. https://doi.org/10.48550/arXiv.2407.03182.

Bestenlehner, J. M., Crowther, P. A., Broos, P. S., Pollock, A. M. T., and Townsley, L. K. (2022) Melnick 33Na: a very massive colliding-wind binary system in 30 Doradus. *MNRAS*, **510**(4), 6133–6149. https://doi.org/10.1093/mnras/stab3521.

Brandi, E., Gosset, E., and Swings, J.-P. (1987) The ultraviolet spectrum of the peculiar emission-line star GG Carinae. *A&A*, **175**(1-2), 151–163. https://ui.adsabs.harvard.edu/abs/1987A&A...175..151B.

Castor, J. I., Abbott, D. C., and Klein, R. I. (1975) Radiation-driven winds in Of stars. *ApJ*, **195**(1), 157–174. https://doi.org/10.1086/153315.

Curé, M. and Araya, I. (2023) Radiation-driven wind hydrodynamics of massive stars: A review. *Galaxies*, **11**(3), 68. https://doi.org/10.3390/galaxies11030068.

Damineli, A., Hillier, D. J., Corcoran, M. F., Stahl, O., Groh, J. H., Arias, J., Teodoro, M., Morrell, N., Gamen, R., Gonzalez, F., Leister, N. V., Levato, H., Levenhagen, R. S., Grosso, M., Colombo, J. F. A., and Wallerstein, G. (2008) A multispectral view of the periodic events in η Carinae. *MNRAS*, **386**(4), 2330–2344. https://doi.org/10.1111/j.1365-2966.2008.13214.x.

Damineli, A., Kaufer, A., Wolf, B., Stahl, O., Lopes, D. F., and de Araújo, F. X. (2000) η Carinae: Binarity confirmed. *ApJL*, **528**(2), L101–L104. https://doi.org/10.1086/312441.

Davidson, K. and Humphreys, R. M. (1997) Eta Carinae and its environment. *ARA&A*, **35**, 1–32. https://doi.org/10.1146/annurev.astro.35.1.1.

Davidson, K. and Humphreys, R. M. (editors) (2012) *Eta Carinae and the Supernova Impostors*, *Astrophysics and Space Science Library*, volume 384. Springer, New York (US-NY). https://doi.org/10.1007/978-1-4614-2275-4.

Davidson, K., Ishibashi, K., and Martin, J. C. (2017) Concerning the orbit of η Car. *RNAAS*, **1**(1), 6. https://doi.org/10.3847/2515-5172/aa96b3.

De Marco, O. and Izzard, R. G. (2017) Dawes Review 6: The impact of companions on stellar evolution. *PASA*, **34**, e001. https://doi.org/10.1017/pasa.2016.52.

Eichler, D. and Usov, V. (1993) Particle acceleration and nonthermal radio emission in binaries of early-type stars. *ApJ*, **402**(1), 271–279. https://doi.org/10.1086/172130.

Ekström, S. (2021) Massive star modelling and nucleosynthesis. *Frontiers in Astronomy and Space Sciences*, **8**, 53. https://doi.org/10.3389/fspas.2021.617765.

Eldridge, J. J. (2017) Population synthesis of massive close binary evolution. In *Handbook of Supernovae*, edited by Alsabti, A. W. and Murdin, P., chapter 27, pages 671–692. Springer, Cham (CH). https://doi.org/10.1007/978-3-319-21846-5_125.

Eldridge, J. J., McClelland, L. A. S., Xiao, L., Stanway, E. R., and Bray, J. (2015) The importance of getting single-star and binary physics correct. In *Wolf–Rayet Stars*, edited by Hamann, W.-R., Sander, A., and Todt, H., pages 177–182. Potsdam University Press, Potsdam (DE). http://nbn-resolving.de/urn:nbn:de:kobv:517-opus4-84268.

Farrell, E., Groh, J. H., Meynet, G., and Eldridge, J. J. (2022) Numerical experiments to help understand cause and effect in massive star evolution. *MNRAS*, **512**(3), 4116–4135. https://doi.org/10.1093/mnras/stac538.

Folini, D. and Walder, R. (2000) 3D hydrodynamical simulations of colliding wind binaries: Theory confronts observations. *Ap&SS*, **274**(1-2), 189–194. https://doi.org/10.1023/A:1026560309386.

Folini, D. and Walder, R. (2002) Theoretical predictions for the cold part of the colliding-wind interaction-zone. In *Interacting Winds from Massive Stars*, edited by Moffat, A. F. J. and St-Louis, N., *Astronomical Society of the Pacific Conference Series*, volume 260, pages 605–614. https://ui.adsabs.harvard.edu/abs/2002ASPC..260..605F.

Garofali, K., Levesque, E. M., Massey, P., and Williams, B. F. (2019) The first candidate colliding-wind binary in M33. *ApJ*, **880**(1), 8. https://doi.org/10.3847/1538-4357/ab286e.

Georgy, C., Hirschi, R., and Ekström, S. (2017) Massive star evolution: What we do (not) know. In *Second BRITE-Constellation Science Conference: Small Satellites – Big Science*, edited by Zwintz, K. and Poretti, E., *Proceedings of the Polish Astronomical Society*, volume 5, pages 37–44. https://www.pta.edu.pl/proc/v5p37.

Gomez, H. L., Vlahakis, C., Stretch, C. M., Dunne, L., Eales, S. A., Beelen, A., Gomez, E. L., and Edmunds, M. G. (2010) Submillimetre variability of Eta Carinae: cool dust within the outer ejecta. *MNRAS*, **401**(1), L48–L52. https://doi.org/10.1111/j.1745-3933.2009.00784.x.

Gosset, E., Hutsemékers, D., Surdej, J., and Swings, J. P. (1985) Radial velocities along the light curve of the peculiar emission-line star GG Carinae. *A&A*, **153**, 71–78. https://ui.adsabs.harvard.edu/abs/1985A&A...153...71G.

Grant, D., Blundell, K., Godden, E., Lee, S., and McCowage, C. (2023) Tracing the colliding winds of η Carinae in He I. *MNRAS*, **526**(4), 6155–6167. https://doi.org/10.1093/mnras/stad3045.

Gull, T. R., Hartman, H., Corcoran, M. F., Damineli, A., Madura, T., Moffat, A. F. J., Richardson, N. D., and Weigelt, G. (2024) Eta Carinae left a curious ladder to climb. arXiv e-prints: arXiv:2403.13954. https://doi.org/10.48550/arXiv.2403.13954.

Hainich, R., Rühling, U., Todt, H., Oskinova, L. M., Liermann, A., Gräfener, G., Foellmi, C., Schnurr, O., and Hamann, W.-R. (2014) The Wolf–Rayet stars in the Large Magellanic Cloud: A comprehensive analysis of the WN class. *A&A*, **565**, A27. https://doi.org/10.1051/0004-6361/201322696.

Hamaguchi, K., Corcoran, M. F., Gull, T., Ishibashi, K., Pittard, J. M., Hillier, D. J., Damineli, A., Davidson, K., Nielsen, K. E., and Kober, G. V. (2007) X-ray spectral variation of η Carinae through the 2003 X-ray minimum. *ApJ*, **663**(1), 522–542. https://doi.org/10.1086/518101.

Heger, A., Langer, N., and Woosley, S. E. (2000) Presupernova evolution of rotating massive stars. I. Numerical method and evolution of the internal stellar structure. *ApJ*, **528**(1), 368–396. https://doi.org/10.1086/308158.

Hillier, D. J., Davidson, K., Ishibashi, K., and Gull, T. (2001) Eta Carinae: The central star. In *Eta Carinae and Other Mysterious Stars: The Hidden Opportunities of Emission Spectroscopy*, edited by Gull, T. R., Johannson, S., and Davidson, K., *Astronomical Society of the Pacific Conference Series*, volume 242, pages 15–28. https://ui.adsabs.harvard.edu/abs/2001ASPC..242...15H.

Hillier, D. J., Koenigsberger, G., Nazé, Y., Morrell, N., Barbá, R. H., and Gamen, R. (2019) The enigmatic binary system HD 5980. *MNRAS*, **486**(1), 725–742. https://doi.org/10.1093/mnras/stz808.

Hirai, R., Podsiadlowski, Ph., Owocki, S. P., Schneider, F. R. N., and Smith, N. (2021) Simulating the formation of η Carinae's surrounding nebula through unstable triple evolution and stellar merger-induced eruption. *MNRAS*, **503**(3), 4276–4296. https://doi.org/10.1093/mnras/stab571.

Humphreys, R. M., Davidson, K., and Smith, N. (1999) η Carinae's second eruption and the light curves of the η Carinae variables. *PASP*, **111**(763), 1124–1131. https://doi.org/10.1086/316420.

Humphreys, R. M., Gordon, M. S., Martin, J. C., Weis, K., and Hahn, D. (2017) Luminous and variable stars in M31 and M33. IV. Luminous Blue Variables, candidate LBVs, B[e] supergiants, and the warm hypergiants: How to tell them apart. *ApJ*, **836**(1), 64. https://doi.org/10.3847/1538-4357/aa582e.

Ishibashi, K., Gull, T. R., Davidson, K., Smith, N., Lanz, T., Lindler, D., Feggans, K., Verner, E., Woodgate, B. E., Kimble, R. A., Bowers, C. W., Kraemer, S., Heap, S. R., Danks, A. C., Maran, S. P., Joseph, C. L., Kaiser, M. E., Linsky, J. L., Roesler, F., and Weistrop, D. (2003) Discovery of a Little Homunculus within the Homunculus Nebula of Carinae. *AJ*, **125**(6), 3222–3236. https://doi.org/10.1086/375306.

Ishii, T., Matsuda, T., Shima, E., Livio, M., Anzer, U., and Boerner, G. (1993) Numerical simulations of two-dimensional and three-dimensional wind accretion flows of an isothermal gas. *ApJ*, **404**, 706. https://doi.org/10.1086/172324.

Kashi, A. (2010) Luminous Blue Variable eruptions triggered and powered by binary interaction. In *International Conferenceon Binaries: ın Celebration of Ron Webbink's 65th Birthday*, edited by Kalogera, V. and van der Sluys, M., *AIP Conference Proceedings*, volume 1314, pages 55–56. AIP Publishing. https://doi.org/10.1063/1.3536411.

Kashi, A. (2017) Accretion at the periastron passage of Eta Carinae. *MNRAS*, **464**(1), 775–782. https://doi.org/10.1093/mnras/stw2303.

Kashi, A. (2019) Simulating the response of the secondary star of Eta Carinae to mass accretion at periastron passage. *MNRAS*, **486**(1), 926–935. https://doi.org/10.1093/mnras/stz837.

Kashi, A. (2020) Wind collision and accretion simulations of the massive binary system HD 166734. *MNRAS*, **492**(4), 5261–5270. https://doi.org/10.1093/mnras/staa203.

Kashi, A. (2023) Accretion in the binary system GG Carinae and implications for B[e] supergiants. *MNRAS*, **523**(4), 5876–5886. https://doi.org/10.1093/mnras/stad1758.

Kashi, A., Davidson, K., and Humphreys, R. M. (2016) Recovery from giant eruptions in very massive stars. *ApJ*, **817**(1), 66. https://doi.org/10.3847/0004-637X/817/1/66.

Kashi, A. and Michaelis, A. (2021) Numerical study of colliding winds in massive stars. *Galaxies*, **10**(1), 4. https://doi.org/10.3390/galaxies10010004.

Kashi, A., Michaelis, A., and Kaminetsky, Y. (2022) Accretion in massive colliding-wind binaries and the effect of the wind momentum ratio. *MNRAS*, **516**(3), 3193–3205. https://doi.org/10.1093/mnras/stac1912.

Kashi, A., Principe, D. A., Soker, N., and Kastner, J. H. (2021) The X-ray properties of Eta Carinae during its 2020 X-ray minimum. *ApJ*, **914**(1), 47. https://doi.org/10.3847/1538-4357/abfa9c.

Kashi, A. and Soker, N. (2007) Modelling the radio light curve of η Carinae. *MNRAS*, **378**(4), 1609–1618. https://doi.org/10.1111/j.1365-2966.2007.11908.x.

Kashi, A. and Soker, N. (2008) Accretion onto the companion of Eta Carinae during the spectroscopic event. V: The infrared decline. *NewA*, **13**(8), 569–580. https://doi.org/10.1016/j.newast.2008.03.003.

Kashi, A. and Soker, N. (2009) Possible implications of mass accretion in Eta Carinae. *NewA*, **14**(1), 11–24. https://doi.org/10.1016/j.newast.2008.04.003.

Kashi, A. and Soker, N. (2010) Periastron passage triggering of the 19th century eruptions of Eta Carinae. *ApJ*, **723**(1), 602–611. https://doi.org/10.1088/0004-637X/723/1/602.

Kashi, A. and Soker, N. (2016) Orbital parameters for the $250\,M_{\odot}$ Eta Carinae binary system. *ApJ*, **825**(2), 105. https://doi.org/10.3847/0004-637X/825/2/105.

Koenigsberger, G., Morrell, N., Hillier, D. J., Gamen, R., Schneider, F. R. N., González-Jiménez, N., Langer, N., and Barbá, R. (2014) The HD 5980 multiple system: Masses and evolutionary status. *AJ*, **148**(4), 62. https://doi.org/10.1088/0004-6256/148/4/62.

Kraus, M. (2019) A census of B[e] supergiants. *Galaxies*, **7**(4), 83. https://doi.org/10.3390/galaxies7040083.

Kraus, M., Borges Fernandes, M., and de Araújo, F. X. (2010) Neutral material around the B[e] supergiant star lha 115-S 65: An outflowing disk or a detached Keplerian rotating disk? *A&A*, **517**, A30. https://doi.org/10.1051/0004-6361/200913964.

Kraus, M., Cidale, L. S., Arias, M. L., Maravelias, G., Nickeler, D. H., Torres, A. F., Borges Fernandes, M., Aret, A., Curé, M., Vallverdú, R., and Barbá, R. H. (2016) Inhomogeneous molecular ring around the B[e] supergiant lha 120-S 73. *A&A*, **593**, A112. https://doi.org/10.1051/0004-6361/201628493.

Kraus, M., Liimets, T., Moiseev, A., Sánchez Arias, J. P., Nickeler, D. H., Cidale, L. S., and Jones, D. (2021) Resolving the circumstellar environment of the Galactic B[e] supergiant star MWC 137.II. Nebular kinematics and stellar variability. *AJ*, **162**(4), 150. https://doi.org/10.3847/1538-3881/ac1355.

Kraus, M., Oksala, M. E., Nickeler, D. H., Muratore, M. F., Borges Fernandes, M., Aret, A., Cidale, L. S., and de Wit, W. J. (2013) Molecular emission from GG Carinae's circumbinary disk. *A&A*, **549**, A28. https://doi.org/10.1051/0004-6361/201220442.

Kudritzki, R.-P. and Puls, J. (2000) Winds from hot stars. *ARA&A*, **38**, 613–666. https://doi.org/10.1146/annurev.astro.38.1.613.

Langer, N. (2012) Presupernova evolution of massive single and binary stars. *ARA&A*, **50**, 107–164. https://doi.org/10.1146/annurev-astro-081811-125534.

Lépine, S. and Moffat, A. F. J. (1999) Wind inhomogeneities in Wolf–Rayet stars. II. ınvestigation of emission-line profile variations. *ApJ*, **514**(2), 909–931. https://doi.org/10.1086/306958.

Liimets, T., Kraus, M., Moiseev, A., Duronea, N., Cidale, L. S., and Fariña, C. (2022) Follow-up of extended shells around B[e] stars. *Galaxies*, **10**(2), 41. https://doi.org/10.3390/galaxies10020041.

Livio, M., Soker, N., de Kool, M., and Savonije, G. J. (1986) Accretion from an inhomogeneous medium – III. General case and observational consequences. *MNRAS*, **222**(2), 235–250. https://doi.org/10.1093/mnras/222.2.235.

Machado, M. A., Araújo, F. X. d., Lopes, D. d. F., and Pereira, C. B. (2004) Using high resolution data to investigate the variability of GG Carinae system. In *IAU Colloquium 194 – Compact Binaries in the Galaxy and Beyond*, edited by Tovmassian, G. and Sion, E., *RMxAA Conference Series*, volume 20, page 239. http://www.astroscu.unam.mx/rmaa/RMxAC..20/PDF/RMxAC..20_mmachado.pdf.

Madura, T. I., Gull, T. R., Owocki, S. P., Groh, J. H., Okazaki, A. T., and Russell, C. M. P. (2012) Constraining the absolute orientation of η Carinae's binary orbit: a 3D dynamical model for the broad [Fe III] emission. *MNRAS*, **420**(3), 2064–2086. https://doi.org/10.1111/j.1365-2966.2011.20165.x.

Maeder, A. (2009) *Physics, Formation and Evolution of Rotating Stars*. Springer, Berlin, Heidelberg (DE), xxi+832 pages. https://doi.org/10.1007/978-3-540-76949-1.

Mahy, L., Lanthermann, C., Hutsemékers, D., Kluska, J., Lobel, A., Manick, R., Miszalski, B., Reggiani, M., Sana, H., and Gosset, E. (2022) Multiplicity of Galactic luminous blue variable stars. *A&A*, **657**, A4. https://doi.org/10.1051/0004-6361/202040062.

Maravelias, G., Kraus, M., Cidale, L. S., Borges Fernandes, M., Arias, M. L., Curé, M., and Vasilopoulos, G. (2018) Resolving the kinematics of the discs around Galactic B[e] supergiants. *MNRAS*, **480**(1), 320–344. https://doi.org/10.1093/mnras/sty1747.

Marston, A. P. and McCollum, B. (2008) Extended shells around B[e] stars: ımplications for B[e] star evolution. *A&A*, **477**(1), 193–202. https://doi.org/10.1051/0004-6361:20066086.

Martin, J. C., Davidson, K., Humphreys, R. M., Hillier, D. J., and Ishibashi, K. (2006) On the He II emission in η Carinae and the origin of its spectroscopic events. *ApJ*, **640**(1), 474–490. https://doi.org/10.1086/500038.

Mason, B. D., Hartkopf, W. I., Gies, D. R., Henry, T. J., and Helsel, J. W. (2009) The high angular resolution multiplicity of massive stars. *AJ*, **137**(2), 3358–3377. https://doi.org/10.1088/0004-6256/137/2/3358.

Mehner, A., Davidson, K., Humphreys, R. M., Walter, F. M., Baade, D., de Wit, W. J., Martin, J., Ishibashi, K., Rivinius, T., Martayan, C., Ruiz, M. T., and Weis, K. (2015) Eta Carinae's 2014.6 spectroscopic event: Clues to the long-term recovery from its Great Eruption. *A&A*, **578**, A122. https://doi.org/10.1051/0004-6361/201425522.

Morris, P. W., Gull, T. R., Hillier, D. J., Barlow, M. J., Royer, P., Nielsen, K., Black, J., and Swinyard, B. (2017) η Carinae's dusty homunculus nebula from near-infrared to submillimeter wavelengths: Mass, composition, and evidence for fading opacity. *ApJ*, **842**(2), 79. https://doi.org/10.3847/1538-4357/aa71b3.

Mukhij, B. and Kashi, A. (in prep.) Accretion and recovery in giant eruptions of massive stars.

Nagae, T., Oka, K., Matsuda, T., Fujiwara, H., Hachisu, I., and Boffin, H. M. J. (2004) Wind accretion in binary stars: I. Mass accretion ratio. *A&A*, **419**(1), 335–343. https://doi.org/10.1051/0004-6361:20040070.

Nazé, Y., Gosset, E., Mahy, L., and Parkin, E. R. (2017) An X-ray view of HD 166734, a massive supergiant system. *A&A*, **607**, A97. https://doi.org/10.1051/0004-6361/201630303.

Nazé, Y., Koenigsberger, G., Pittard, J. M., Parkin, E. R., Rauw, G., Corcoran, M. F., and Hillier, D. J. (2018) A changing wind collision. *ApJ*, **853**(2), 164. https://doi.org/10.3847/1538-4357/aaa29c.

Nugis, T. and Lamers, H. J. G. L. M. (2000) Mass-loss rates of Wolf–Rayet stars as a function of stellar parameters. *A&A*, **360**, 227–244. https://ui.adsabs.harvard.edu/abs/2000A&A...360..227N.

Oskinova, L. M., Hamann, W.-R., and Feldmeier, A. (2007) Neglecting the porosity of hot-star winds can lead to underestimating mass-loss rates. *A&A*, **476**(3), 1331–1340. https://doi.org/10.1051/0004-6361:20066377.

Oudmaijer, R. D. and Miroshnichenko, A. S. (2017) Introduction to the B[e] phenomenon. In *The B[e] Phenomenon: Forty Years of Studies*, edited by Miroshnichenko, A., Zharikov, S., Korčáková, D., and Wolf, M., *Astronomical Society of the Pacific Conference Series*, volume 508, pages 3–10. http://aspbooks.org/custom/publications/paper/508-0003.html.

Owocki, S. (2010) Hot-star mass-loss mechanisms: Winds and outbursts. In *Hot and Cool: Bridging Gaps in Massive Star Evolution*, edited by Leitherer, C., Bennett, P. D., Morris, P. W., and Van Loon, J. T., *Astronomical Society of the Pacific Conference Series*, volume 425, pages 199–208. http://aspbooks.org/custom/publications/paper/425-0199.html.

Owocki, S. (2011) Theory of winds from hot, luminous massive stars. *BSRSL*, **80**, 16–28. https://popups.uliege.be/0037-9565/index.php?id=2478.

Owocki, S. P. (2015) Instabilities in the envelopes and winds of very massive stars. In *Very Massive Stars in the Local Universe*, edited by Vink, J. S., *Astrophysics and Space Science Library*, volume 412, chapter 5, pages 113–156. Springer, Cham (CH). https://doi.org/10.1007/978-3-319-09596-7_5.

Parkin, E. R., Pittard, J. M., Corcoran, M. F., and Hamaguchi, K. (2011) Spiraling out of control: Three-dimensional hydrodynamical modeling of the colliding winds in η Carinae. *ApJ*, **726**(2), 105. https://doi.org/10.1088/0004-637X/726/2/105.

Paxton, B., Cantiello, M., Arras, P., Bildsten, L., Brown, E. F., Dotter, A., Mankovich, C., Montgomery, M. H., Stello, D., Timmes, F. X., and Townsend, R. (2013) Modules for Experiments in Stellar Astrophysics (MESA): Planets, oscillations, rotation, and massive stars. *ApJS*, **208**(1), 4. https://doi.org/10.1088/0067-0049/208/1/4.

Paxton, B., Marchant, P., Schwab, J., Bauer, E. B., Bildsten, L., Cantiello, M., Dessart, L., Farmer, R., Hu, H., Langer, N., Townsend, R. H. D., Townsley, D. M., and Timmes, F. X. (2015) Modules for Experiments in Stellar Astrophysics (MESA): Binaries, pulsations, and explosions. *ApJS*, **220**(1), 15. https://doi.org/10.1088/0067-0049/220/1/15.

Podsiadlowski, Ph. (2010) Massive binary evolution. *NewAR*, **54**(3-6), 39–44. https://doi.org/10.1016/j.newar.2010.09.023.

Pollock, A. M. T., Crowther, P. A., Tehrani, K., Broos, P. S., and Townsley, L. K. (2018) The 155-day X-ray cycle of the very massive Wolf– Rayet star Melnick 34 in the Large Magellanic Cloud. *MNRAS*, **474**(3), 3228–3236. https://doi.org/10.1093/mnras/stx2879.

Porter, A., Blundell, K., and Lee, S. (2022) The circumbinary rings of GG Carinae: indications of disc eccentricity growth in the B[e] supergiant's atomic emission lines. *MNRAS*, **509**(2), 1720–1735. https://doi.org/10.1093/mnras/stab3083.

Porter, A., Grant, D., Blundell, K., and Lee, S. (2021) GG Carinae: orbital parameters and accretion indicators from phase-resolved spectroscopy and photometry. *MNRAS*, **501**(4), 5554–5574. https://doi.org/10.1093/mnras/staa3749.

Puls, J., Markova, N., Scuderi, S., Stanghellini, C., Taranova, O. G., Burnley, A. W., and Howarth, I. D. (2006) Bright OB stars in the Galaxy. III. Constraints on the radial stratification of the clumping factor in hot star winds from a combined H_α, IR and radio analysis. *A&A*, **454**(2), 625–651. https://doi.org/10.1051/0004-6361:20065073.

Puls, J., Vink, J. S., and Najarro, F. (2008) Mass loss from hot massive stars. *A&ARv*, **16**(3-4), 209–325. https://doi.org/10.1007/s00159-008-0015-8.

Quataert, E., Fernández, R., Kasen, D., Klion, H., and Paxton, B. (2016) Super-Eddington stellar winds driven by near-surface energy deposition. *MNRAS*, **458**(2), 1214–1233. https://doi.org/10.1093/mnras/stw365.

Richardson, N. D., Gies, D. R., Gull, T. R., Moffat, A. F. J., and St-Jean, L. (2015) The optical wind line variability of η Carinae during the 2009.0 event. *AJ*, **150**(4), 109. https://doi.org/10.1088/0004-6256/150/4/109.

Ruffert, M. (1994) Three-dimensional hydrodynamic Bondi–Hoyle accretion. I. Code validation and stationary accretors. *ApJ*, **427**, 342–350. https://doi.org/10.1086/174144.

Sana, H., de Mink, S. E., de Koter, A., Langer, N., Evans, C. J., Gieles, M., Gosset, E., Izzard, R. G., Le Bouquin, J.-B., and Schneider, F. R. N. (2012) Binary interaction dominates the evolution of massive stars. *Sci*, **337**, 444–446. https://doi.org/10.1126/science.1223344.

Schneider, F. R. N., Podsiadlowski, Ph., and Laplace, E. (2024) Pre-supernova evolution and final fate of stellar mergers and accretors of binary mass transfer. *A&A*, **686**, A45. https://doi.org/10.1051/0004-6361/202347854.

Schrøder, S. L., MacLeod, M., Ramirez-Ruiz, E., Mandel, I., Fragos, T., Loeb, A., and Everson, R. W. (2021) The evolution of binaries under the influence of radiation-driven winds from a stellar companion. arXiv e-prints: arXiv:2107.09675. https://doi.org/10.48550/arXiv.2107.09675.

Shenar, T., Sana, H., Marchant, P., Pablo, B., Richardson, N., Moffat, A. F. J., Van Reeth, T., Barbá, R. H., Bowman, D. M., Broos, P., Crowther, P. A., Clark, J. S., de Koter, A., de Mink, S. E., Dsilva, K., Gräfener, G., Howarth, I. D., Langer, N., Mahy, L., Maíz Apellániz, J., Pollock, A. M. T., Schneider, F. R. N., Townsley, L., and Vink, J. S. (2021) The Tarantula massive binary monitoring: V. R 144: a wind-eclipsing binary with a total mass $\gtrsim 140 M_\odot$. *A&A*, **650**, A147. https://doi.org/10.1051/0004-6361/202140693.

Smartt, S. J. (2009) Progenitors of core-collapse supernovae. *ARA&A*, **47**, 63–106. https://doi.org/10.1146/annurev-astro-082708-101737.

Smith, N. (2014) Mass loss: Its effect on the evolution and fate of high-mass stars. *ARA&A*, **52**, 487–528. https://doi.org/10.1146/annurev-astro-081913-040025.

Smith, N. and Tombleson, R. (2015) Luminous blue variables are antisocial: their isolation implies that they are kicked mass gainers in binary evolution. *MNRAS*, **447**(1), 598–617. https://doi.org/10.1093/mnras/stu2430.

Soker, N. (2001) The departure of η Carinae from axisymmetry and the binary hypothesis. *MNRAS*, **325**(2), 584–588. https://doi.org/10.1046/j.1365-8711.2001.04439.x.

Soker, N. (2005) Accretion by the secondary in η Carinae during the spectroscopic event. I. Flow parameters. *ApJ*, **635**(1), 540–546. https://doi.org/10.1086/497389.

Soker, N. and Behar, E. (2006) Accretion onto the companion of η Carinae during the spectroscopic event. III. The He II λ4686 line. *ApJ*, **652**(2), 1563–1571. https://doi.org/10.1086/508336.

Soker, N., Livio, M., de Kool, M., and Savonije, G. J. (1986) Accretion of angular momentum from an inhomogeneous medium – II. ısothermal flow. *MNRAS*, **221**(2), 445–452. https://doi.org/10.1093/mnras/221.2.445.

Stevens, I. R., Blondin, J. M., and Pollock, A. M. T. (1992) Colliding winds from early-type stars in binary systems. *ApJ*, **386**, 265–287. https://doi.org/10.1086/171013.

Sundqvist, J. O., Puls, J., and Feldmeier, A. (2010) Mass loss from inhomogeneous hot star winds: I. Resonance line formation in 2D models. *A&A*, **510**, A11. https://doi.org/10.1051/0004-6361/200912842.

Swings, J. P. (1974) Similarities in the spectra of three southern peculiar emission line stars with infrared excesses: HD 45677, HD 87643 and GG Carinae (HD 94878). *A&A*, **34**, 333–334. https://ui.adsabs.harvard.edu/abs/1974A&A....34..333S.

Tehrani, K. A., Crowther, P. A., Bestenlehner, J. M., Littlefair, S. P., Pollock, A. M. T., Parker, R. J., and Schnurr, O. (2019) Weighing Melnick 34: the most massive binary system known. *MNRAS*, **484**(2), 2692–2710. https://doi.org/10.1093/mnras/stz147.

Torres, A. F., Cidale, L. S., Kraus, M., Arias, M. L., Barbá, R. H., Maravelias, G., and Borges Fernandes, M. (2018) Resolving the clumpy circumstellar environment of the B[e] supergiant LHA 120-S 35. *A&A*, **612**, A113. https://doi.org/10.1051/0004-6361/201731723.

Usov, V. V. (1992) Stellar wind collision and X-ray generation in massive binaries. *ApJ*, **389**, 635–648. https://doi.org/10.1086/171236.

van Marle, A. J., Owocki, S. P., and Shaviv, N. J. (2008) Numerical simulations of continuum-driven winds of super-Eddington stars. *MNRAS*, **389**(3), 1353–1359. https://doi.org/10.1111/j.1365-2966.2008.13648.x.

van Marle, A. J., Owocki, S. P., and Shaviv, N. J. (2009) On the behaviour of stellar winds that exceed the photon-tiring limit. *MNRAS*, **394**(2), 595–604. https://doi.org/10.1111/j.1365-2966.2008.14366.x.

Vanbeveren, D., De Donder, E., Van Bever, J., Van Rensbergen, W., and De Loore, C. (1998) The WR and O-type star population predicted by massive star evolutionary synthesis. *NewA*, **3**(7), 443–492. https://doi.org/10.1016/S1384-1076(98)00020-7.

Vink, J. S. (2015) Mass-loss rates of very massive stars. In *Very Massive Stars in the Local Universe*, edited by Vink, J. S., *Astrophysics and Space Science Library*, volume 412, chapter 4, pages 77–111. Springer, Cham (CH). https://doi.org/10.1007/978-3-319-09596-7_4.

Vink, J. S. (2022) Theory and diagnostics of hot star mass loss. *ARA&A*, **60**, 203–246. https://doi.org/10.1146/annurev-astro-052920-094949.

Vishniac, E. T. (1994) Nonlinear instabilities in shock-bounded slabs. *ApJ*, **428**(1), 186–208. https://doi.org/10.1086/174231.

Walder, R. and Folini, D. (2000) On the stability of colliding flows: Radiative shocks, thin shells, and supersonic turbulence. *Ap&SS*, **274**(1-2), 343–352. https://doi.org/10.1023/A:1026597318472.

Walder, R. and Folini, D. (2002) Theoretical considerations on colliding clumped winds. In *Interacting Winds from Massive Stars*, edited by Moffat, A. F. J. and St-Louis, N., *Astronomical Society of the Pacific Conference Series*, volume 260, pages 595–604. http://www.aspbooks.org/a/volumes/article_details/?paper_id=24448.

Walder, R. and Folini, D. (2003) 3D-hydrodynamics of colliding winds in massive binaries. In *A Massive Star Odyssey: From Main Sequence to Supernova*, edited by van der Hucht, K., Herrero, A., and Esteban, C., *Symposium – International Astronomical Union*, volume 212, pages 139–147. https://doi.org/10.1017/S0074180900211741.

Weis, K. (2011) Nebulae around Luminous Blue Variables – large bipolar variety. *Proceedings of the International Astronomical Union*, **6**(S272), 372–377. https://doi.org/10.1017/S1743921311010799.

Weis, K. and Bomans, D. J. (2020) Luminous blue variables. *Galaxies*, **8**(1), 20. https://doi.org/10.3390/galaxies8010020.

Williams, P. M., Morrell, N. I., Boutsia, K., and Massey, P. (2021) The episodic dust-making Wolf–Rayet star HD 38030 in the Large Magellanic Cloud. *MNRAS*, **505**(4), 5029–5037. https://doi.org/10.1093/mnras/stab1625.

Zapartas, E., de Mink, S. E., Justham, S., Smith, N., Renzo, M., and de Koter, A. (2021) Effect of binary evolution on the inferred initial and final core masses of hydrogen-rich, Type II supernova progenitors. *A&A*, **645**, A6. https://doi.org/10.1051/0004-6361/202037744.

Zickgraf, F.-J. (2006) B[e] supergiants in the Magellanic Clouds. In *Stars with the B[e] Phenomenon*, edited by Kraus, M. and Miroshnichenko, A. S., *Astronomical Society of the Pacific Conference Series*, volume 355, pages 135–145. http://aspbooks.org/custom/publications/paper/355-0135.html.

Zickgraf, F.-J., Humphreys, R. M., Lamers, H. J. G. L. M., Smolinski, J., Wolf, B., and Stahl, O. (1996) Spectroscopic study of the outflowing disk winds of B[e] supergiants in the Magellanic Clouds. *A&A*, **315**, 510–520. https://ui.adsabs.harvard.edu/abs/1996A&A...315..510Z.

Zickgraf, F.-J., Wolf, B., Stahl, O., Leitherer, C., and Appenzeller, I. (1986) B(e)-supergiants of the Magellanic Clouds. *A&A*, **163**, 119–134. https://ui.adsabs.harvard.edu/abs/1986A&A...163..119Z.